

Mineralogy and crystal chemistry of a low grade nickel laterite ore

ZHU De-qing¹, CUI Yu¹, Sarath HAPUGODA², Keith VINING², PAN Jian¹

1. School of Minerals Processing and Bioengineering, Central South University, Changsha 410083, China;

2. Process Science and Engineering, Commonwealth Scientific and Industrial Research Organization,
P.O. Box 883, Kenmore QLD 4069, Australia

Received 19 April 2011; accepted 26 August 2011

Abstract: To acquire understanding of Ni enrichment from laterite ore, the mineralogy and crystal chemistry of a low grade limonite type nickel laterite ore sample assaying 0.97% Ni from Indonesia were studied using optical microscopy, X-ray diffraction (XRD), scanning electron microscopy (SEM) and electron probe microanalysis (EPMA). According to EPMA results, the mineral includes 80% goethite ((Fe, Ni, Al)O(OH)) with 0.87% Ni, 15% silicate minerals with lizardite ((Mg, Fe, Ni)₃Si₂O₅(OH)) and olivine ((Mg, Fe, Ni)₂SiO₄), and 1.19% Ni, and other minor phases, such as hematite, maghemite, chromite and quartz, and no Ni was detected. The mineralogy of the laterite ore indicates that due to the complicated association of the various phases and the variable distribution of Ni, this refractory laterite ore can not be upgraded by traditional physical beneficiation processes.

Key words: nickel laterite; crystal chemistry; nickel occurrence; goethite; lizardite

1 Introduction

As an important metal, nickel is widely used in stainless steel and new material industries. According to marketing observations, 66.2% of the total metal nickel is consumed by the stainless steel industry [1]. Rapid expansion of these industries, especially stainless steel manufacture, dramatically has increased the demand for nickel in recent years [2]. Of all the land nickel reserves, 30% exists as sulfide ores with the balance comprised of oxide ores. The oxide ores are typically referred to as nickel laterite ores [3]. In traditional nickel industries, about 60% of the metal nickel was produced from sulfide ores about ten years ago [4]. However, miners of nickel sulfide ores have been confronted with increasing challenges due to much deeper drilling requirements, higher production costs and more depleting reserves. Therefore, nickel laterite ore has attracted greater attention in recent years, leading to about 50% of metal nickel being produced from laterite currently [5,6]. China has become the largest nickel consumer in the world due to soaring production of stainless steel. More nickel

laterite ores are imported into China because of the depletion of domestic nickel sulfide resources. Consequently, it is of great importance to the Chinese economy to effectively utilize low grade nickel laterite ore [7].

Nickel laterite ores are formed by the weathering of olivine bedrock in tropical to sub-tropical climates [8,9]. There are some previous studies on the mineralogy of nickel laterite ores from New Caledonian, Cuba, Greece, Turkey, Africa, India and Australia, but little work is found on Indonesia laterite ores. The association of metals such as Mg, Ni, Mn and Co with goethite has been rigorously studied by previous researchers [10], but fewer studies have been completed on the metals association within low grade laterite ore. In this work, low grade nickel laterite sample from Indonesia for a subsequent Ni enrichment mechanism was studied to understand the association of Ni.

2 Experimental

2.1 Nickel laterite ore sample

A low grade nickel laterite ore sample from

Indonesia was selected for the study. The chemical composition is listed in Table 1 and the loss on ignition is 13.23%. Polished blocks were prepared from representative sub-samples of the ore using the analytical techniques. Due to the soft and friable nature of the ore, the sample was crushed to size of 4 mm to ensure the adequate quality of polished blocks.

Table 1 Chemical composition of nickel laterite ore sample (mass fraction, %)

Fe	FeO	Ni	Co	Cr ₂ O ₃	MnO
40.09	1.14	0.97	0.089	2.86	0.82
SiO ₂	Al ₂ O ₃	CaO	MgO	S	P
12.55	6.52	0.3	4.65	0.035	0.0063

2.2 Method

A Zeiss Axiophot optical microscope at CSIRO Process Science and Engineering's Brisbane laboratory, Australia was used to observe the microstructure and an Axio Vision 4.6 was used for image acquiring. XRD analysis was carried out on a D/MAX2500X X-ray diffractometer at Changsha Research Institute of Mining and Metallurgy, China. Scanning electron microscopy and electron probe micro analysis tests were carried out at University of Queensland, Australia. Scanning electron microscopy (SEM) including backscatter electron imaging (BSE), energy dispersive X-ray spectrometry (EDAX) and micro beam spot chemical analyses were carried out for several representative ore samples. The analyses were carried out using a JEOL superprobe microanalyser, model JXA-8200L.

For the analyses, representative particles of the ore material were set in an epoxy resin mount, which was then sectioned to expose the sample before being polished using successively finer diamond paste, down to a final cutting size of 1 μm. The sample was then coated with a 25–30 nm thick carbon film prior to analysis. All the polished resin mounts were examined under the optical microscope equipped with a digital image acquiring system and connected to a personal computer. The image acquiring software AXIO Vision was used to optimize and save the digital images. Different ore minerals and associated gangue minerals present were identified under the optical microscope. These optical images were used as basic guide maps for electron probe micro-analyzer (EPMA). The EPMA analyses were carried out in the Centre for Microscopy and Microanalysis (CMM) at the University of Queensland, using a JEOL Super Probe 8800L equipped with wavelength-dispersive spectrometer. The micro-probe was operated with an accelerating voltage of 15 kV,

current of 15 nA and spot size from 0 to 5 μm, and counting time was 30 s for major elements and 40 s for trace elements. The analysis of standard samples was conducted first to calibrate the results.

3 Results and discussion

3.1 Mineral composition

The XRD pattern of the laterite ore sample is shown in Fig. 1 and the result indicates that goethite ((Fe, Ni, Al)O(OH)) accounts for 80%, silicate minerals (lizardite ((Mg, Fe, Ni)₃Si₂O₅(OH)) and olivine ((Mg, Fe, Ni)₂SiO₄)) account for about 15% of the total phases in the sample. Other trace minerals include chromite ((Fe, Mg)O(Cr, Fe, Al)₂O₃), hematite (Fe₂O₃), maghemite, quartz and asbolane. According to all of the analytical results, no independent nickel minerals were observed, which is consistent with other researchers [11]. The porous structure of goethite and silicates during the weathering and leaching process absorbs nickel randomly, so nickel could not be upgraded effectively by traditional beneficiation processes due to the low Ni grade.

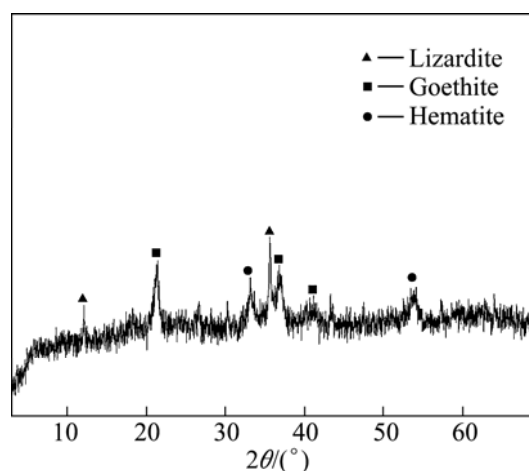


Fig. 1 XRD pattern of laterite ore sample

3.2 Goethite

As the dominant phase, most goethite particles are closely associated with silicate minerals, chromite, quartz and maghemite, as shown in Fig. 2. Two types of goethite structures are observed in this study, earthy goethite and vitreous goethite. Earthy goethite is recognized for its fine grained and friable nature, and vitreous goethite is recognized due to its hard and compact nature. In Fig. 2(a), earthy goethite with minor hematite is the main phase, whilst in Fig. 2 (c) hematite (point 1), silicate (point 3), chromite (point 4) and quartz (point 5) are observed embedded in earthy

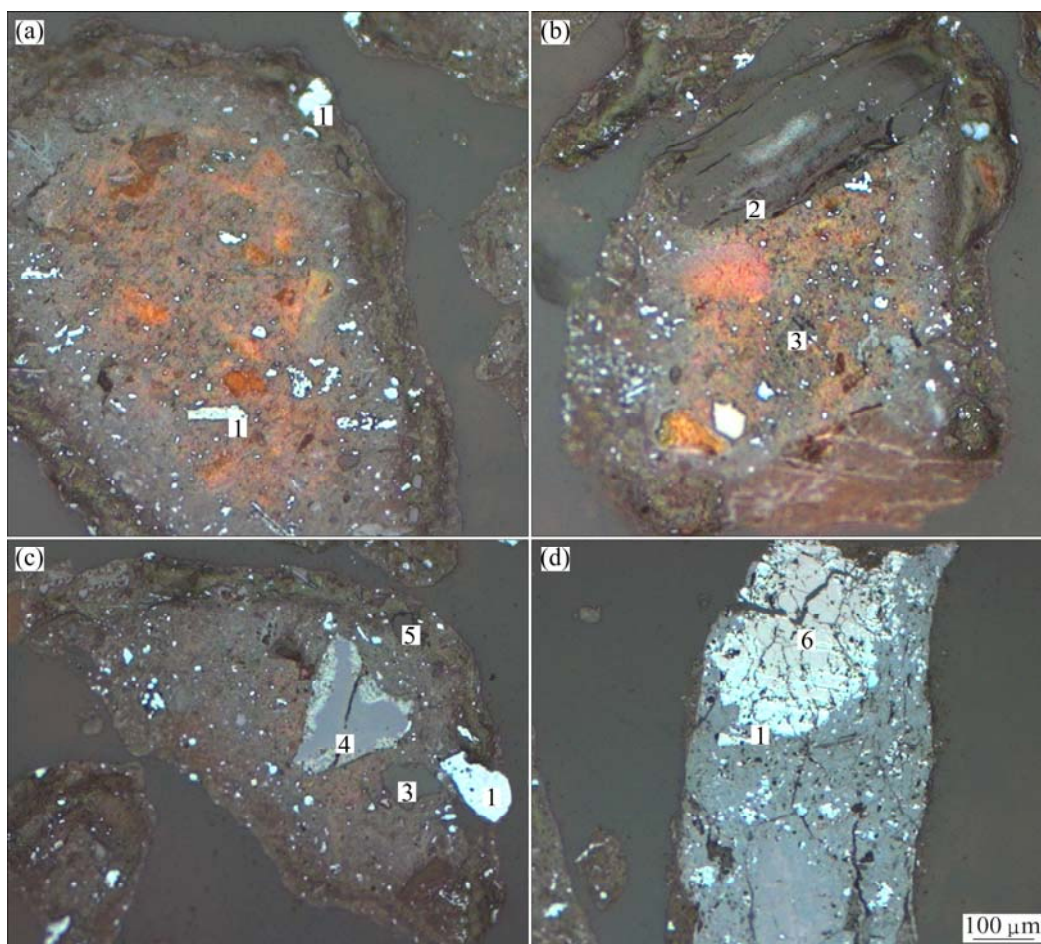


Fig. 2 OM images showing complex structure of goethite in laterite sample including earthy goethite associated with hematite (a), lizardite (b), chromite (c) and vitreous goethite (d) (1—Hematite; 2—Lizardite; 3—Silicate; 4—Chromite; 5—Quartz; 6—Magnetite)

goethite. Vitreous goethite occurs in rectangular structures with hematite, chromite, silicate minerals and magnemite inclusions, as shown in Fig. 2(d).

Figure 3 illustrates the earthy goethite structure using optical microscopy and SEM backscatter image-BSE, respectively. Areas (I) and (II) in Fig. 3(b) are selected for minerals spectroscopic analysis due to the representative structure. The results are shown in Figs. 3(e)–(j). It is observed in the high magnification image (Fig. 3(c)) that the earthy goethite matrix is densely populated with fine grained inclusions of hematite, lizardite and other minerals down to a size of approximately 10 μm. This highlights the requirement for very fine grinding to achieve nickel enrichment through physical separation. In the earthy goethite matrix (point 8), Al and Mg are detected in Fig. 3(e), as well as Fe and O. However, no obvious Ni peak is detected. As shown in Fig. 3(c), goethite (point 3) with size of 20 μm is detected. This goethite particle is associated with strong peaks of Fe, O, Al and Si; and even a weak Ni peak is evident (Fig. 3(h)). Quartz shows high purity in

Fig. 3(i) because of the dense structure. According to other work [12,13], on the limonitic laterite ore, nickel is rich in goethite accompanied by intergrowth of silicate minerals. This is also evident in SEM analysis resulted from Fig. 3(h), wherein Ni and Si both show weak peaks compared with Fig. 3(e).

The EPMA analysis results are shown in Fig. 4 and Table 2. The analyzed areas are marked by the numbers and the line indicates the linear probe analysis trajectory. Silicates and goethite are the two Ni host phases containing 1.19% and 0.82% Ni, respectively. Hematite and quartz components are of high purity. Organic minerals are found in goethite particles at a trace level.

To study the relationship among the inclusion elements in goethite phase, linear elemental analysis was conducted. The results are shown in Figs. 5 and 6. The lines in Figs. 5(a) and (b) and Figs. 6(a) and (b) illustrate the analysis path. Earthy goethite particles in the analyzed areas contain high Ni in association with high Si concentration. Fe varies antithetically with Al concentration, which is consistent with previous research

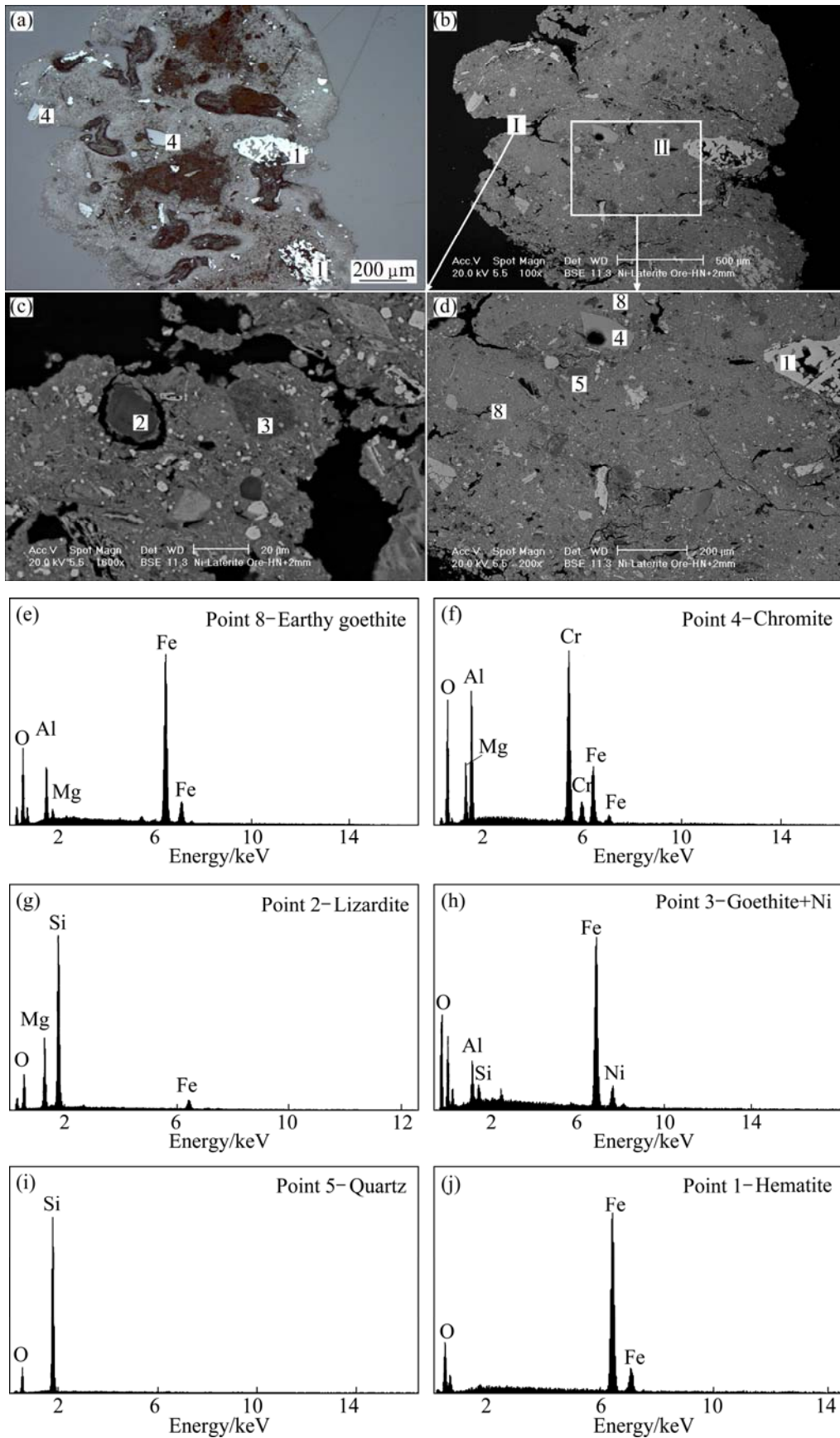


Fig. 3 SEM analyses of earthy goethite particles: (a) Optical image; (b) BSE image in low magnification; (c), (d) BSE image in high magnification; (e)–(j) EDAX spectra

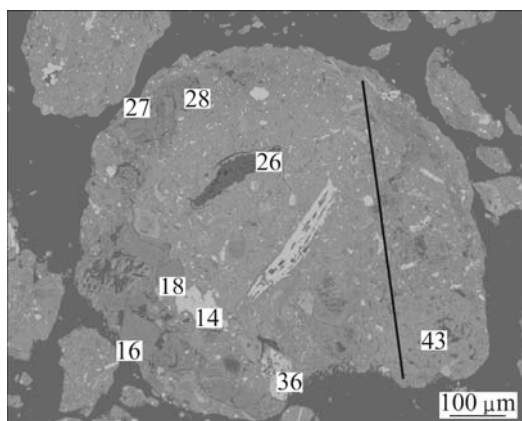


Fig. 4 BSE image of complicated earthy goethite particles under EPMA (16, 18, 27, 28—silicates; 14, 36—hematite; 43—goethite; 26—organic mineral)

work and shows that Al is common to substitute Fe in goethite [14,15]. The common substitution is due to the same valence and comparable ionic radius. All these findings are consistent with previous research on reaction (1) during laterite ore mineralization [11]:



This process occurs under acid conditions that Si^{2+} and Ni^{2+} might deposit in porous goethite, resulting in the similar distribution of Ni and Si which could explain the association behaviors of Ni within earthy goethite.

3.3 Silicate minerals

The microstructure of lizardite particles is illustrated in Fig. 7. Long lizardite particles with a tabular geometry are observed, as shown in Figs. 7(a),

Table 2 Mineral compositions of complicated earthy goethite particles measured by EPMA

Mineral	w(O)/%	w(Ni)/%	w(Co)/%	w(Mg)/%	w(Fe)/%	w(Al)/%	w(Mn)/%	w(Si)/%	Total/%
Silicate	28.44	1.19	0.02	5.29	14.10	0.36	0.02	19.47	69.50
Earthy goethite	23.78	0.82	0.05	0.17	42.19	4.54	0.23	2.08	75.65
Hematite quartz organic	29.44	0.07	0.13	0.20	70.31	0.00	0.18	0.25	98.75
	52.47	0.07	0.03	0.01	0.93	0.01	0.01	41.14	94.79
	9.16	0.04	0.00	0.66	0.52	0.03	0.04	0.00	12.58

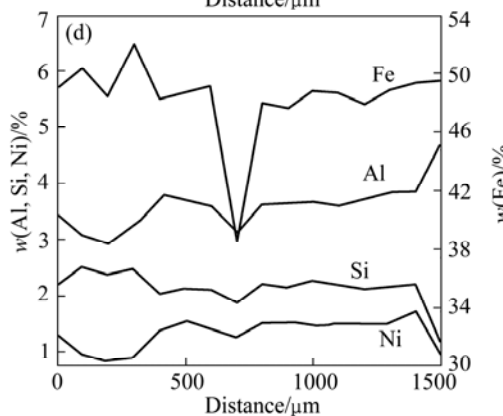
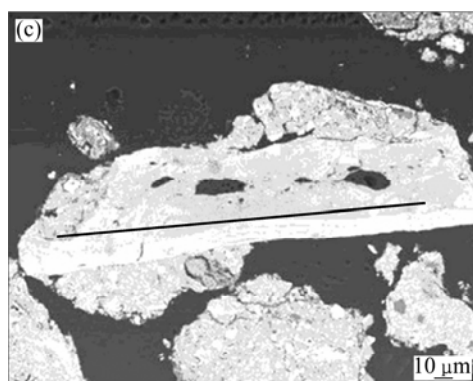
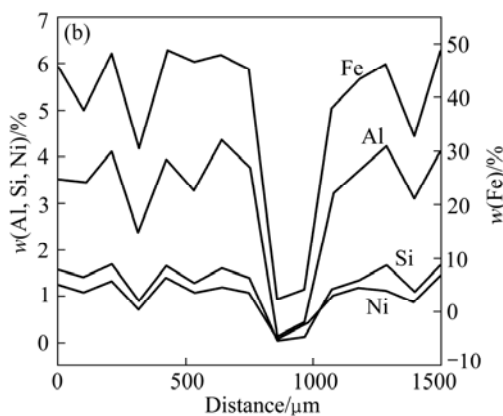
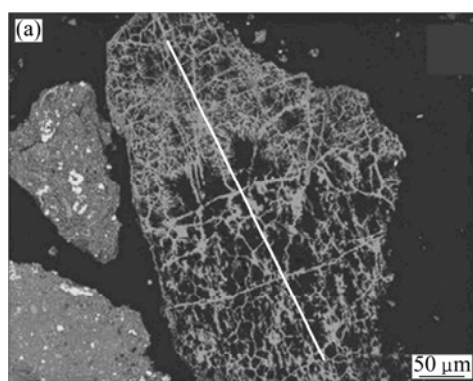


Fig. 5 EPMA analyses of vitreous goethite: (a), (b) BSE image and corresponding elemental analysis of particle 1#; (c), (d) BSE image and corresponding elemental analysis of particle 2#

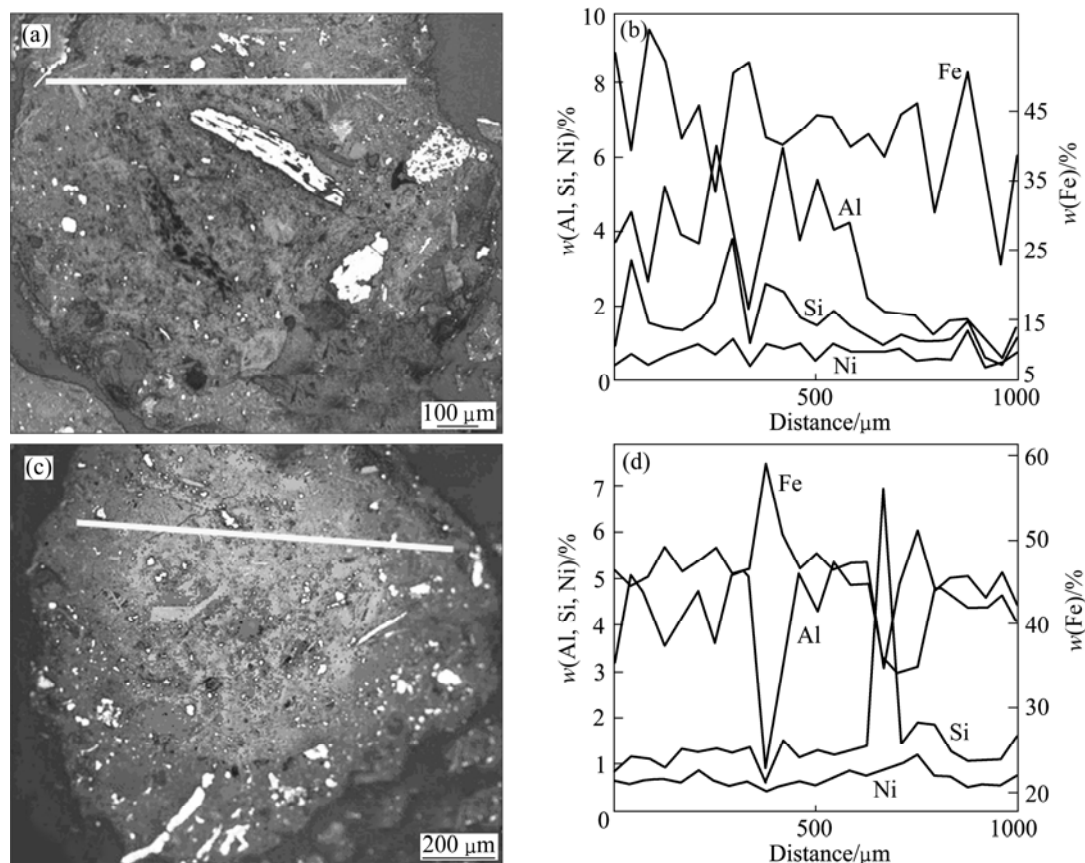
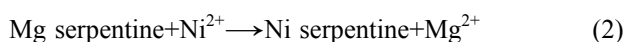


Fig. 6 EPMA analyses of earthy goethite: (a), (b) BSE image and corresponding elemental analysis of particle 3#; (c), (d) BSE images and corresponding elemental analysis of particle 4#

(b), (d), (f) and (g), in contrast to the erratic geometry commonly associated with vein textures in Figs. 7(c), (e) and (h). Lizardite is evident as an independent phase associated with goethite as shown in Figs. 7(f) and (g) and chromite as shown in Fig. 7(h).

Optical and BSE images with associated spectroscopic analyses of lizardite and associated vein quartz are shown in Fig. 8. The detected lizardite appears as dark area in Figs. 8(a) and (b); however, there is associated vein quartz, as shown in Fig. 8(c). Ni is detected at concentration as high as 9% in the lizardite phase, as shown in Fig. 8(d).

The EPMA analysis of lizardite is presented in Fig. 9, in which Fig. 9(b) is taken from the rectangular area in Fig. 9(a) analyzed by EPMA along the line, and the BSE image is shown in Fig. 9(c). Lizardite contains 2.23% Ni and 30% combined water. According to previous studies [11], during the dissolution of serpentine or olivine, reaction (2) occurs:



This reaction illustrates that Ni-bearing silicates in laterite ore are formed due to the ionic exchange

reactions, which is agreed with this study. It is shown in Fig. 9(d) that the silicates broadly possess reverse concentrations of Ni with Mg.

3.4 Other phases

3.4.1 Asbolane

Asbolane could be occasionally found to contain more Ni and Co compared with other Ni-bearing minerals (Fig. 10). Porous asbolane is embedded in earthy goethite, similarly to goethite and lizardite. However, from the optical and BEI images, the asbolane and goethite form aggregates and the obvious interlinkage of the two phases contributes to complex chemical results during the EPMA tests. This is evident from the high iron compositions from asbolane analysis. In contrast to the other mineral components discussed, asbolane contains Co as high as 3.06%. Mn, Fe, Co, Ni, Al and Si contents are plotted in Fig. 10(d). Asbolane is the main Co-bearing phase from this study, and the same results are found from the nickel laterite deposited in Moa Bay area, Cuba. Nickel, cobalt and aluminum are detected accumulating in asbolane [16].

3.4.2 Maghemite, chromite and quartz

Maghemite, chromite and quartz possess a dense

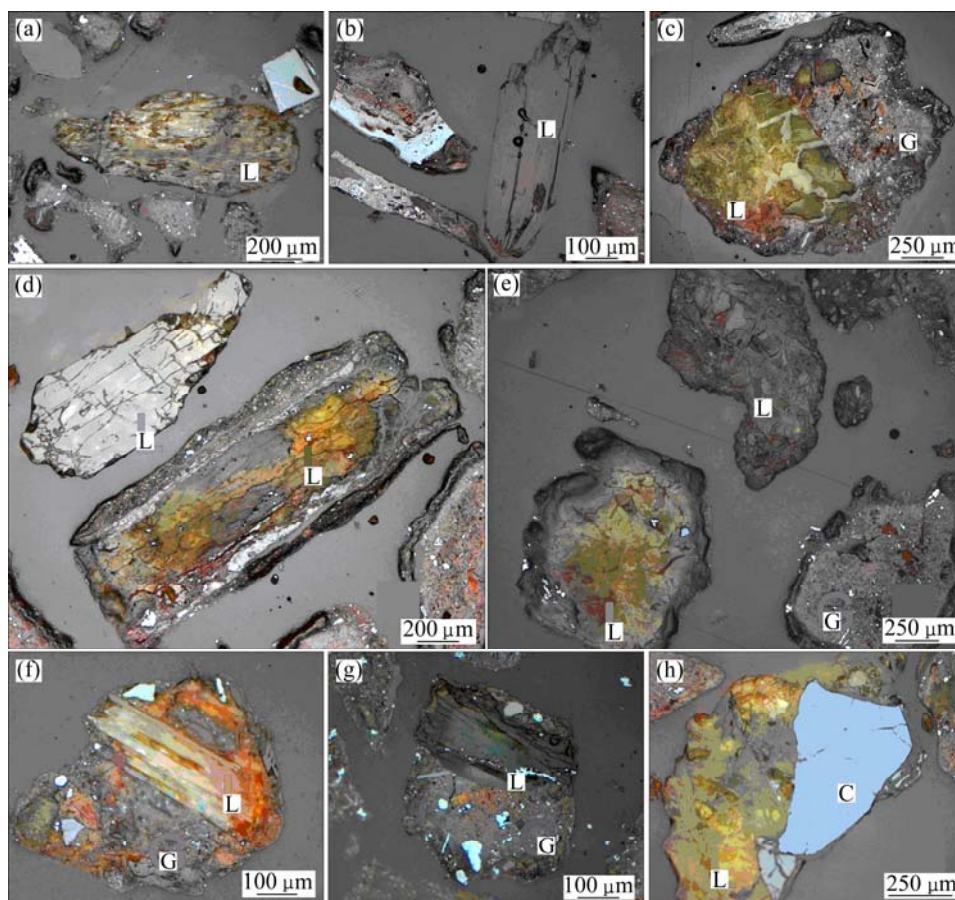


Fig. 7 Optical images of various lizardite of laterite sample: (a), (b) Independent particles; (c), (d), (e), (f), (g) Lizardite associated with goethite; (h) Lizardite associated with chromite (L—lizardite, G—goethite, C—chromite)

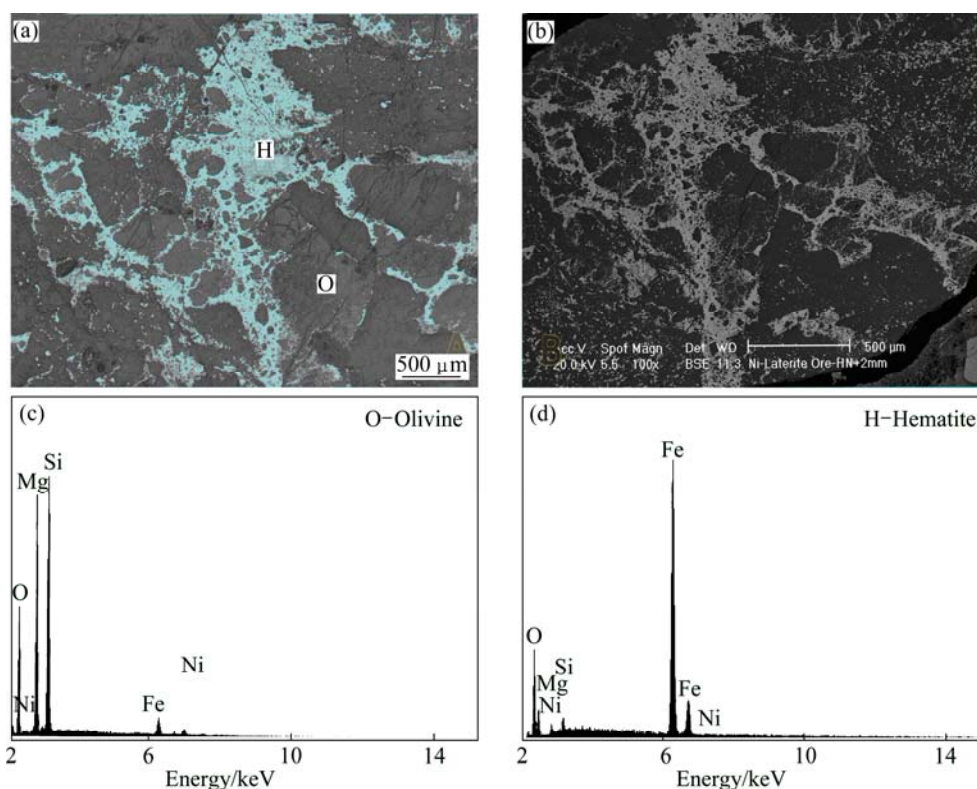


Fig. 8 Microstructures and EDX analyses of lizardite particles: (a) Optical image; (b) BSE image; (c), (d) EDAX spectra

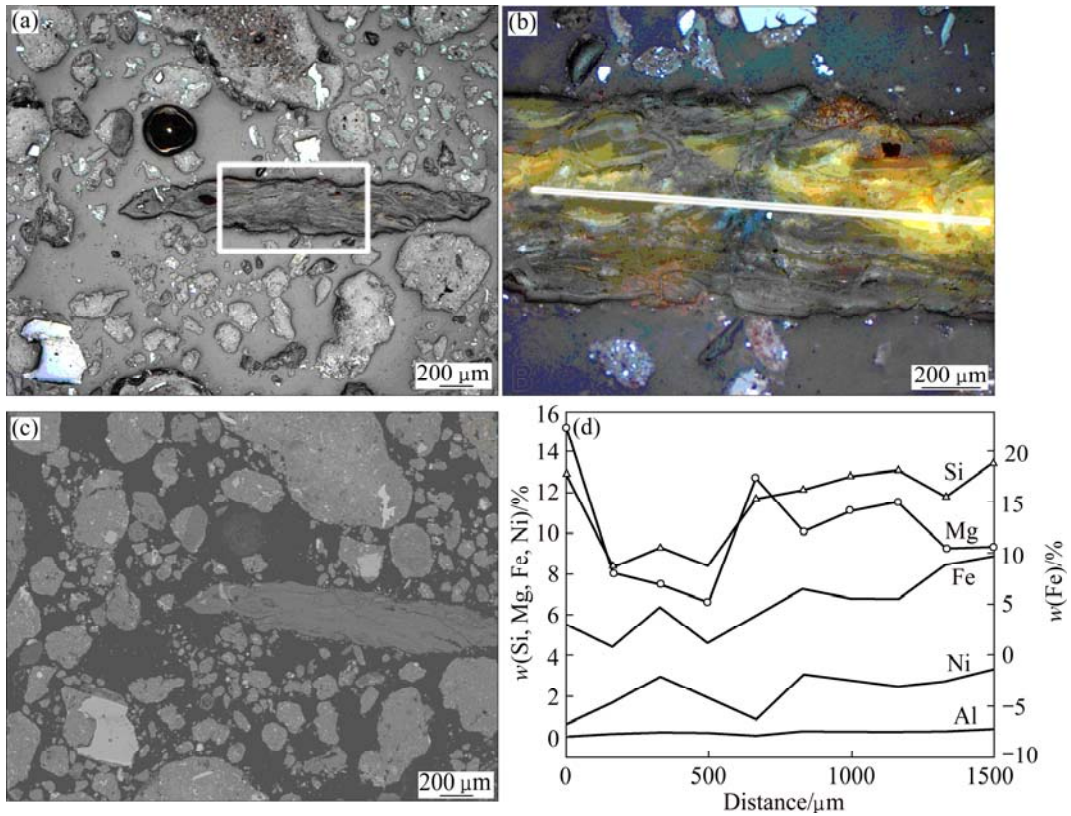


Fig. 9 EPMA analyses of lizardite particles: (a) Optical image in low magnification; (b) Optical image in high magnification; (c) BSE image; (d) Elemental analysis

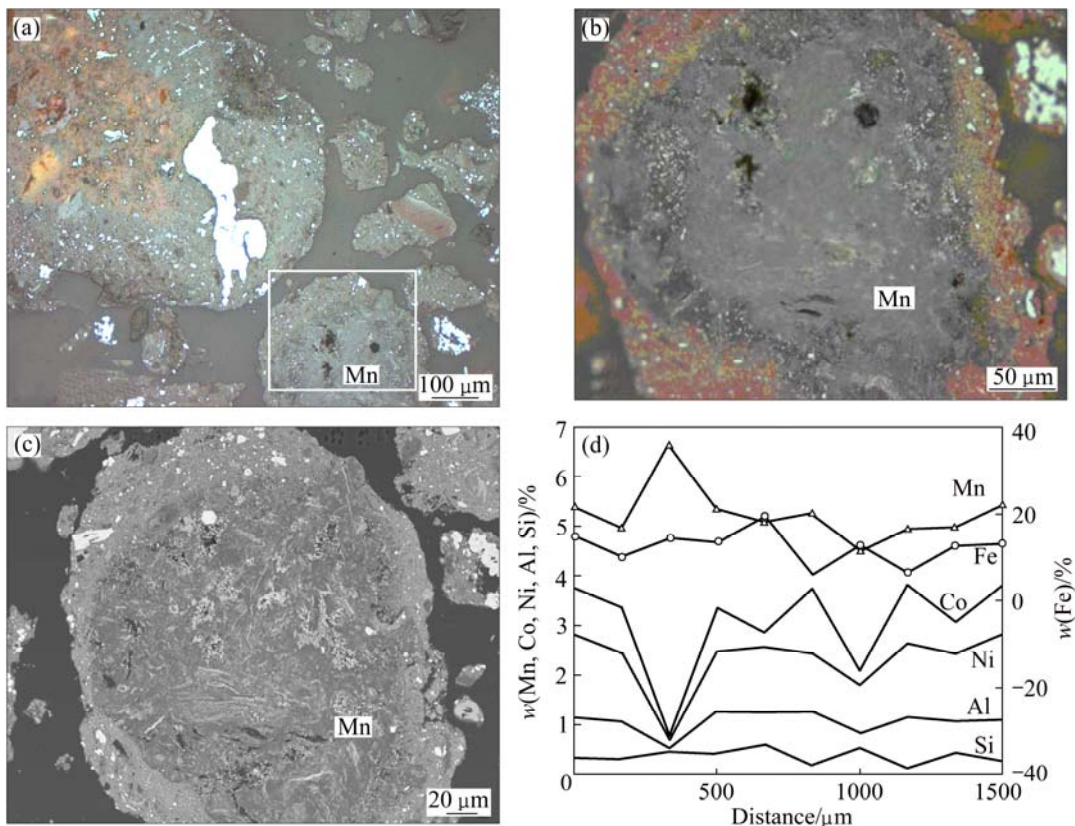


Fig. 10 EPMA analyses of asbolane: (a) Optical image in low magnification; (b) Optical image in high magnification; (c) BSE image; (d) Elemental analysis (Mn–Asbolane)

Table 3 Average compositions of minerals (mass fraction, %)

Mineral	Mineral proportion	O	Ni	Co	Mg	Cr	Fe	Al	Mn	Si	Total
Goethite	77.54	24.55	0.87	0.06	0.28	0.74	44.23	3.79	0.25	1.80	77.06
Asbolane	–	17.14	2.31	3.06	0.33	0.07	12.30	1.08	19.95	0.38	57.46
Silicates	13.43	36.93	1.19	0.02	11.77	0.19	10.55	0.52	0.06	21.12	82.94
Chromite	3.14	33.00	0.06	0.07	5.00	34.43	19.72	6.63	0.41	0.11	99.48
Quartz	0.92	51.24	0.13	0.02	0.20	0.08	2.51	0.06	0.02	41.23	95.53
Hematite	2.96	28.59	0.14	0.11	0.61	0.21	66.55	0.61	0.23	0.18	98.5

structure with smooth surface when polished and could be either observed in close association with goethite and lizardite, or exhibit as independent phases. However, according to SEM and EPMA, no Ni is detected in these phases.

3.5 Compositions of minerals

The EPMA analyses of least 30 points from each main phase measured for element contents and the average results are summarized in Table 3. Asbolane, quartz, hematite and maghemite compositions are at trace levels, and asbolane is listed because it contains high Co.

4 Conclusions

1) The studied laterite sample consists of 80% goethite with porous and soft structure, 15% silicate minerals (lizardite and olivine) and other minor phases, including chromite, maghemite, hematite and quartz, but no independent Ni minerals exist.

2) Goethite and silicates phases are the Ni host phases which contain 0.87% and 1.19% Ni, respectively. Because of the low Ni concentration and variable distribution in these phases, effectively upgrading by physical beneficiation processes would be challenging.

References

- [1] ZAINOL Z. The development of a resin-in-pulp process for the recovery of nickel and cobalt from laterite leach slurries [D]. Perth Australia: Murdoch University, 2005: 2–3.
- [2] MOSKALYK R R, ALFANTAZI A M. Nickel laterite processing and electrowinning practice [J]. *Minerals Engineering*, 2002, 15(8): 593–605.
- [3] AGATZINI-LEONARDOU S, TSAKIRIDIS P E, OUSTADAKIS P, KARIDAKIS T, KATSIAP I A. Hydrometallurgical process for the separation and recovery of nickel from sulphate heap leach liquor of nickeliferous laterite ores [J]. *Minerals Engineering*, 2009, 22(14): 1181–1192.
- [4] BLAKEY B C, JAMES D F. Characterizing the rheology of laterite slurries [J]. *International Journal of Mineral Processing*, 2003, 70(1–4): 23–39.
- [5] PICKLES C A. Microwave heating behaviour of nickeliferous limonitic laterite ores [J]. *Minerals Engineering*, 2004, 17: 775–784.
- [6] MCDONALD R G, WHITTINGTON B I. Atmospheric acid leaching of nickel laterites review Part II. Chloride and bio-technologies [J]. *Hydrometallurgy*, 2008, 91: 56–69.
- [7] ZHU D Q, CUI Y, PAN J, QIU G Z, LI Q H. Investigation on manufacture of ferronickel from low grade nickel laterite by pre-reducing–magnetic separation–smelting process [C]//Science Press. Proceedings of XXIV International Mineral Processing Congress. Beijing: Beijing General Research institute of Mining & Metallurgy, 2008: 1622–1633.
- [8] THORNE R, HERRINGTON R, ROBERTS S. Composition and origin of the Çaldag oxide nickel laterite W Turkey [J]. *Mineralium Deposita*, 2009, 44(3): 581–595.
- [9] YONGUE R, YEMEFACK M, WOUATONG A S L, NDJIGUI P D, BILONG P. Contrasted mineralogical composition of the laterite cover on serpentinites of Nkamouna-Kongo, southeast Cameroon [J]. *Clay Minerals*, 2009, 44(2): 221–237.
- [10] LANDERS M, GILKES R J. Dehydroxylation and dissolution of nickeliferous goethite in New Caledonian lateritic Ni ore [J]. *Applied Clay Science*, 2007, 35(3–4): 162–172.
- [11] ELIAS M, DONALDSON M J, GIORGETTA N. Geology, mineralogy and chemistry of lateritic nickel-cobalt deposits near Kalgoorlie western australia [J]. *Economic Geology*, 1981, 76(4): 1775–1783.
- [12] OLIVERIRA S M B, PARTITI C S M, ENZWEILER J. Ochreous laterite: A nickel ore from Punta Gorda, Cuba [J]. *Journal of South American Earth Sciences*, 2001, 14(3): 307–317.
- [13] ELIOPOULOS D G, ECONOMOU-ELIOPOULOS M. Geochemical and mineralogical characteristics of Fe–Ni and bauxitic-laterite deposits of Greece [J]. *Ore Geology Review*, 2000, 16(1–2): 41–58.
- [14] SINGH B, SHERMAN D M, GILKES R J, WELLS M A, MOSSELMANS J F W. Incorporation of Cr, Mn and Ni into goethite (α -FeOOH): mechanism from extended X-ray absorption fine structure spectroscopy [J]. *Clay Minerals*, 2002, 37(4): 639–649.
- [15] LANDERS M, GILKES R J, WELLS M A. Rapid dehydroxylation of nickeliferous goethite in lateritic nickel ore: X-ray diffraction and TEM investigation [J]. *Clays and Clay Minerals*, 2009, 57(6): 751–770.
- [16] ROGUE-ROSELL J, MOSSELMANS J F W, PROENZA J A, LABRADOR M, GALI S, ATKINSON K D, QUINN P D. Sorption of Ni by “lithiophorite–asbolane” intermediates in moa bay lateritic deposits, eastern Cuba [J]. *Chemical Geology*, 2010, 275(1–2): 9–18.

某印尼低品位红土镍矿的微观结构及晶体化学

朱德庆¹, 崔瑜¹, Sarath HAPUGODA², Keith VINING², 潘建¹

1. 中南大学 资源加工与生物工程学院, 长沙 410083;

2. Process Science and Engineering, Commonwealth Scientific and Industrial Research Organization,
P.O. Box 883, Kenmore QLD 4069, Australia

摘要: 为深入研究红土镍矿的镍富集原理, 利用电子显微镜、扫描电镜、X 射线衍射分析以及电子探针微区分析对含镍 0.97% 的某印尼低品位红土镍矿的工艺矿物学进行研究, 以了解镍钴有价金属的分布及赋存状态。实验表明: 该矿样主要矿物为针铁矿(含量约为 80%), 镍含量约为 0.87%; 含镍、铁、镁的结晶水硅酸盐矿物((Mg, Fe, Ni)₂SiO₄)的含量约为 15%, 如利蛇纹石((Fe, Ni, Al)O(OH))和橄榄石((Mg, Fe, Ni)₃Si₂O₅(OH))等, 镍含量约在 1.19% 左右; 其它含量较低的物相为赤铁矿、磁赤铁矿、铬铁矿和石英等, 这些矿物的镍含量极低。钴土矿是含钴矿物, 分析发现该矿物往往有较高的镍和钴含量。微观检测发现: 红土镍矿微观结构复杂, 不同矿物之间共生普遍, 主要矿物的微观结构松散, 因而传统选矿方式很难实现镍的富集。

关键词: 红土镍矿; 晶体化学; 镍赋存状态; 针铁矿; 利蛇纹石

(Edited by FANG Jing-hua)